**Supporting Information**

# Enhanced visible-light-driven photocatalytic $H_2$ production and Cr(VI) reduction of a $ZnIn_2S_4/MoS_2$ heterojunction synthesized by the biomolecule-assisted microwave heating method

Watcharapong Pudkon[a], Hasliza Bahruji[b], Peter J. Miedziak[b,c], Thomas E. Davies[b], David J. Morgan[b], Samuel Pattisson[b], Sulawan Kaowphong[a,d,e,*], Graham J. Hutchings[b,*]

[a] *Department of Chemistry, Faculty of Science, Chiang Mai University, Chiang Mai 50200, Thailand*

[b] *Cardiff Catalysis Institute, School of Chemistry, Cardiff University, Main Building, Park Place CF10 3AT, Cardiff, UK*

[c]*School of Applied Sciences, University of South Wales, Pontypridd CF37 4AT, UK*

[d]*Environmental Science Research Center (ESRC), Faculty of Science, , Chiang Mai University, Chiang Mai 50200, Thailand*

[e]*Center of Excellence for Innovation in Chemistry, Faculty of Science, Chiang Mai University, Chiang Mai 50200, Thailand*

1. Calculation method for the apparent quantum yield (AQY)

The apparent quantum yield (AQY) of $ZnIn_2S_4$ and $ZnIn_2S_4/MoS_2$-40%wt photocatalysts for the $H_2$ production and Cr(VI) production were calculated according to the following equations:

$$AQY(\%) = \frac{2\ x\ number\ of\ evolved\ H_2\ molecules}{number\ of\ incident\ photon} \times 100$$

where the light intensity is 119.43 mW/cm$^2$ and the irradiated surface area is 12.56 cm$^2$ with a 400 nm band pass filter.

$$AQY(\%) = \frac{3\ x\ number\ of\ reduced\ Cr(VI)\ ions}{number\ of\ incident\ photon} \times 100$$

where the light intensity is 62.20 mW/cm$^2$ and the irradiated surface area is 6.25 cm$^2$ with a 400 nm band pass filter.

2. The procedure of the silver photo-deposition experiment

First, the $ZnIn_2S_4/MoS_2$-40%wt composite (50 mg, 150 mL) was dispersed in the $Ag(NO_3)_2$ solution (1 mM) under visible light irradiation for 360 min. Then, the photocatalyst after photo-depositing Ag was collected, washed several times with DI water and dried (60 $^oC$).

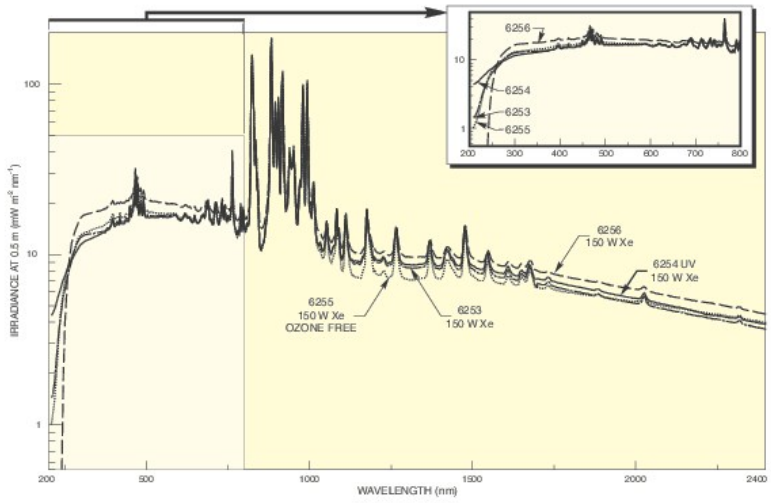


**Fig. S1.** Spectral irradiance of the 150 W Xe lamp (Model 6256, Newport[1,2]).

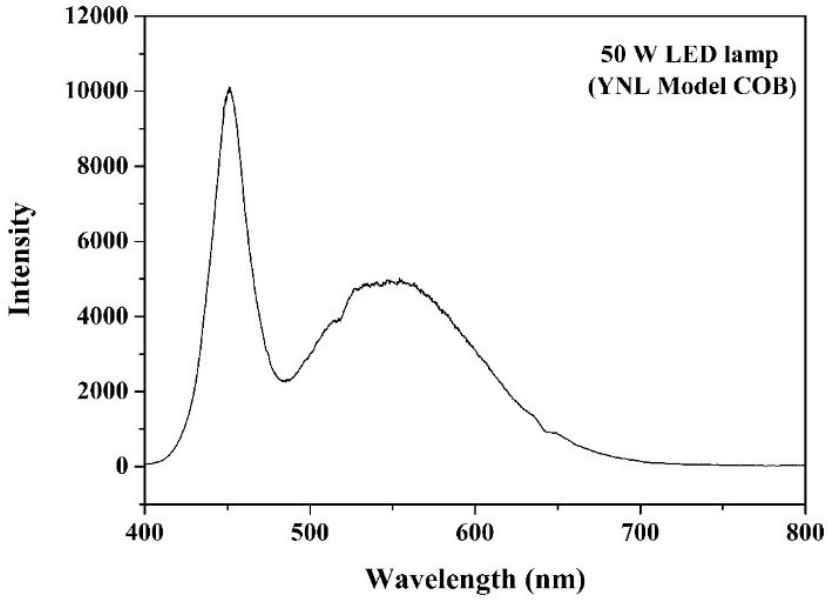


**Fig. S2.** Spectral irradiance of the 50 W LED lamp (YNL Model COB).

[1] https://www.newport.com.cn/medias/sys_master/images/images/hfb/hdf/8797196451870/Light-Sources.pdf

[2] https://www.newport.com.cn/n/information-on-spectral-irradiance-data

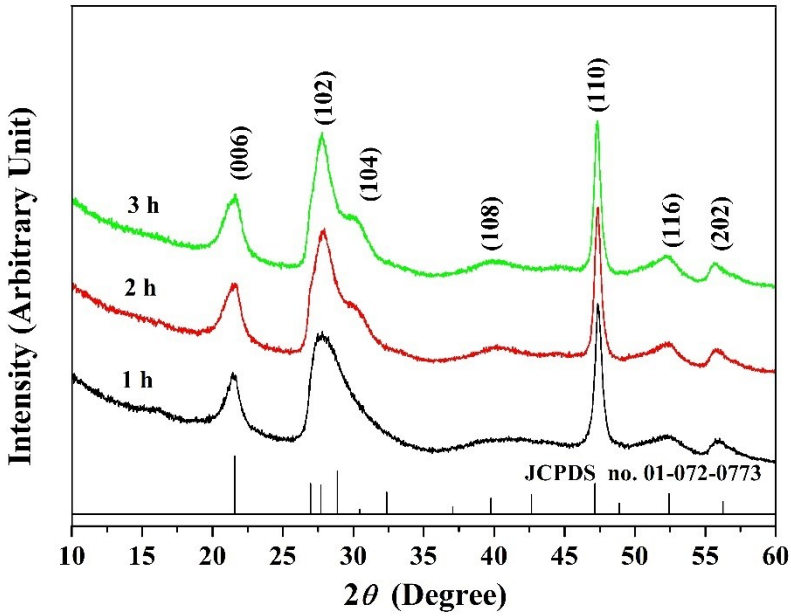


**Fig. S3.** XRD patterns of the $ZnIn_2S_4$ powders synthesized at different microwave heating times.

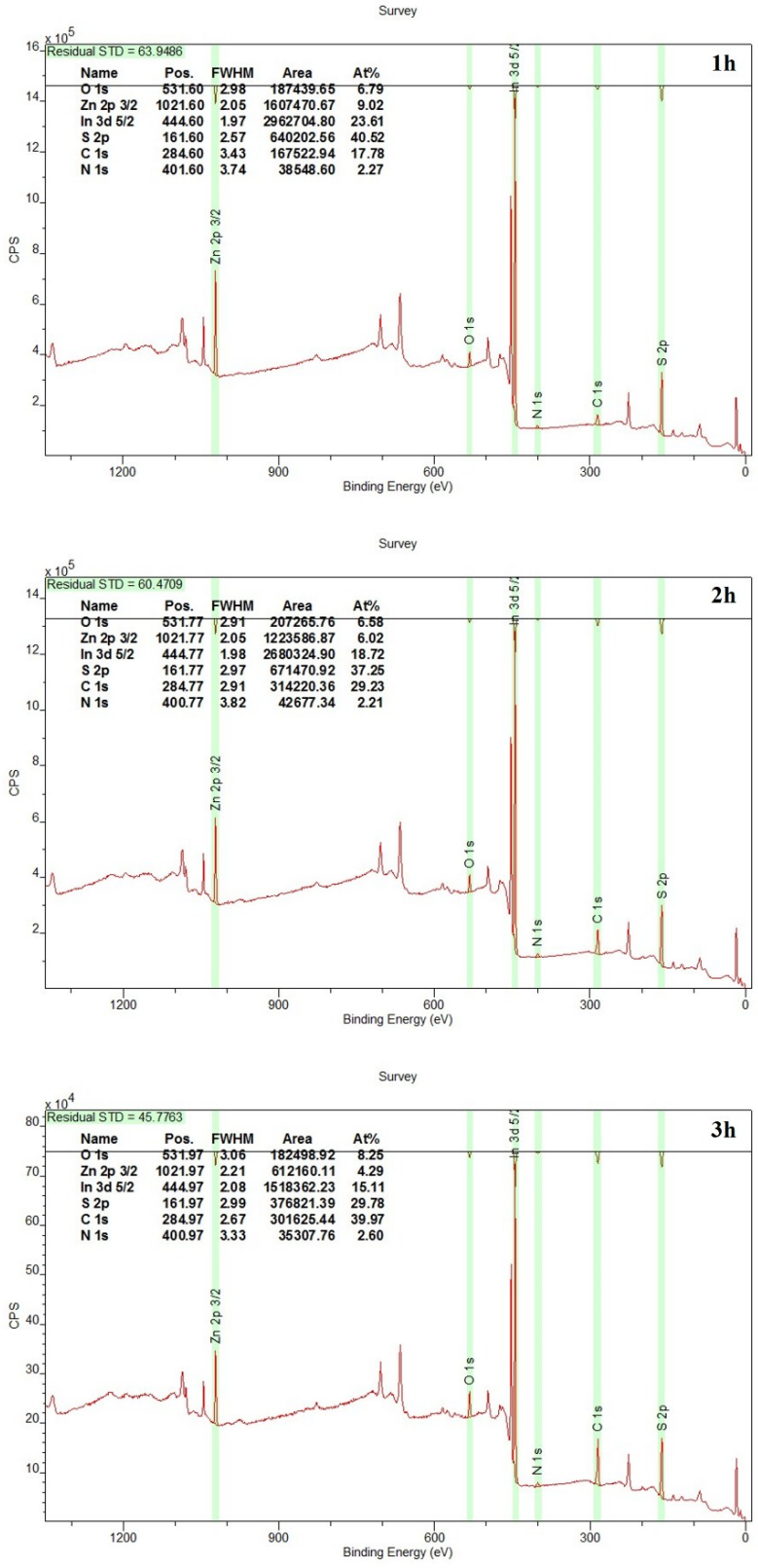


**Fig. S4.** Survey XPS spectra and the detailed chemical compositions of $ZnIn_2S_4$ synthesized at microwave heating time of 1, 2 and 3 h.

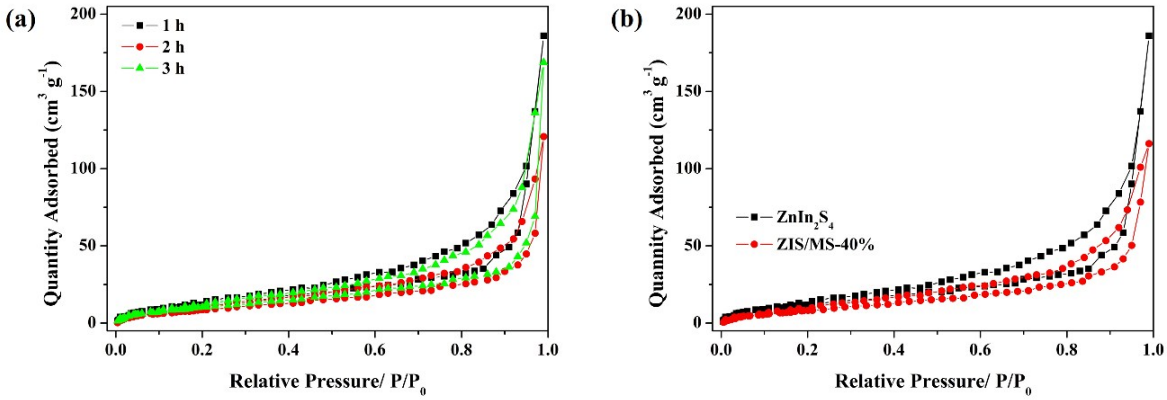


**Fig. S5.** The $N_2$ adsorption-desorption isotherms of **(a)** $ZnIn_2S_4$ synthesized at different microwave heating times, and **(b)** $ZnIn_2S_4/MoS_2$-40%wt compared with that of $ZnIn_2S_4$. All amples exhibit type-IV isotherms with the hysteresis loops in the range of 0.4-1.0 $P/P_0$, indicating the presence of slit-like mesopores due to the stacking of sheets.[3]

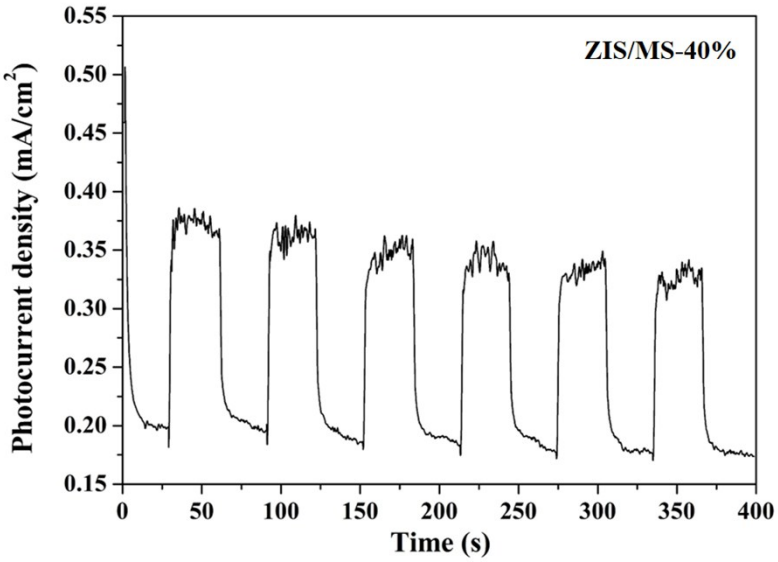


**Fig. S6.** Transient photocurrent density-time curve of the $ZnIn_2S_4/MoS_2$-40%wt photoelectrode.

[3] C.Liu, B. Chai, C. Wang, J. Yan, Z. Ren, Solvothermal fabrication of $MoS_2$ anchored on $ZnIn_2S_4$ microspheres with boosted photocatalytic hydrogen evolution activity, *Inter. J. Hydrogen Energy,* 2018, 43(14), 6977-6986.

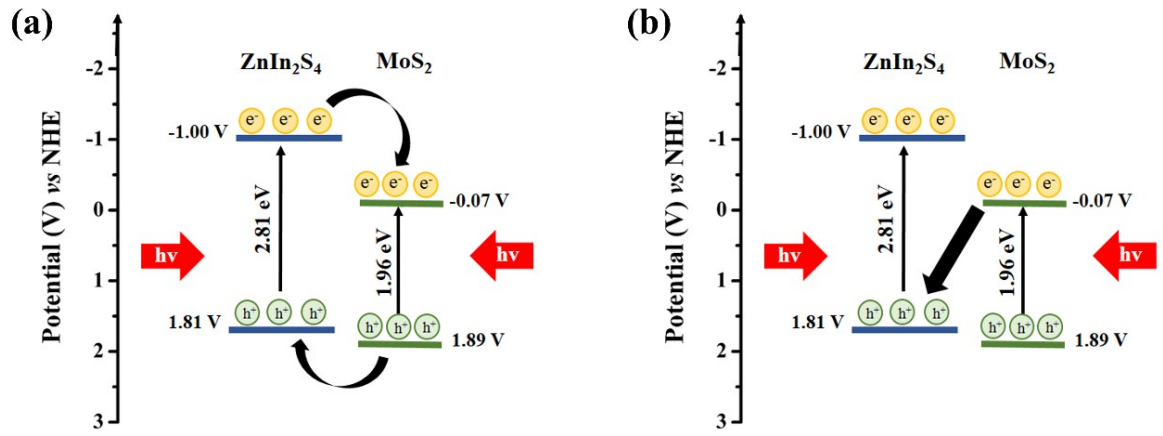


**Fig. S7.** The energy band positions and possible charges transfer in the $ZnIn_2S_4/MoS_2$ photocatalyst through **(a)** conventional type-II heterojunction and **(b)** Z-scheme heterojunction.

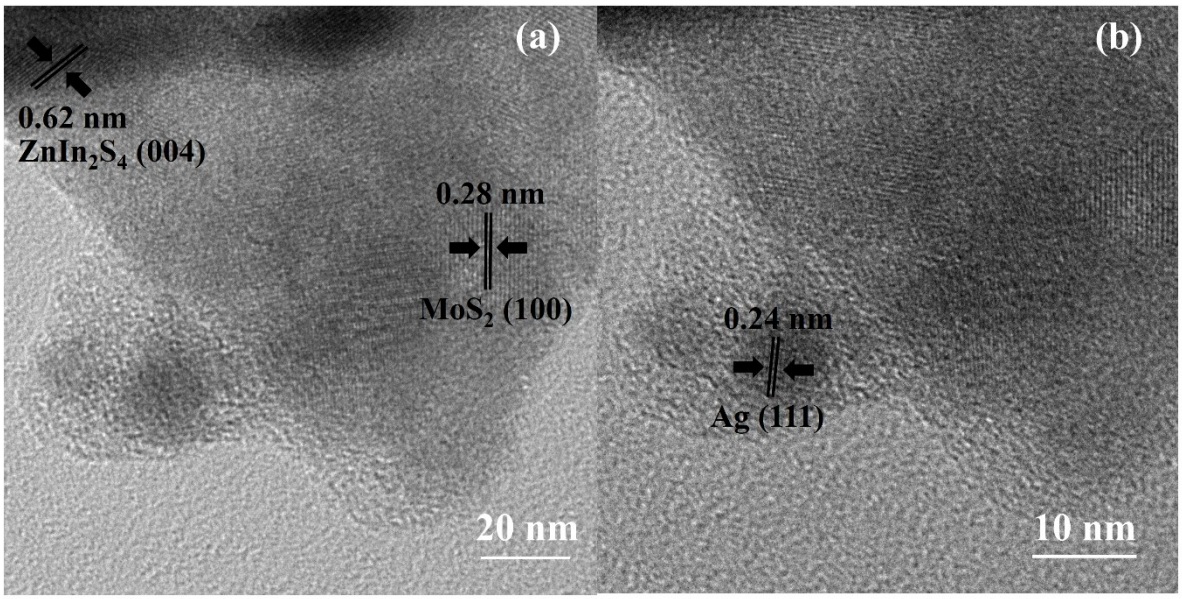


**Fig. S8. (a)-(b)** High-magnified TEM images of the silver nanoparticle deposited on the $MoS_2$ particle in the $ZnIn_2S_4/MoS_2$-40%wt composite. **(b)** Lattice fringe of Ag nanoparticles.

**Table S1.** Fitting parameter ($\chi^2$), amplitudes ($\alpha_1$, $\alpha_2$), excited-state lifetime ($\tau_1$, $\tau_2$), and average exciton lifetime $<\tau>$ for $ZnIn_2S_4$ and $ZnIn_2S_4/MoS_2$-40%wt.

| | $\chi^2$ | $\alpha_1$ | $\alpha_2$ | $\tau_1$ (ns) | $\tau_2$ (ns) | $<\tau>$ (ns) |
|---|---|---|---|---|---|---|
| $ZnIn_2S_4$ | 1.25 | 17.69 | 82.31 | 1.38 | 14.03 | 13.77 |
| $ZnIn_2S_4/MoS_2$-40%wt | 1.22 | 15.65 | 84.35 | 2.53 | 18.20 | 17.81 |

The average lifetime ($<\tau>$) was calculated using the equation[4,5]:

$<\tau> = (\alpha_1\tau_1^2 + \alpha_2\tau_2^2)/(\alpha_1\tau_1 + \alpha_2\tau_2)$

$\chi^2$: the goodness of fit parameter. The ideal $\chi^2$ values are 0.8-1.3.[6]

**Table S2.** The $E_{VB}$ and $E_{CB}$ of $ZnIn_2S_4$ and $MoS_2$ calculated by the Mulliken electronegativity (EN) theory and Mott-Schottky measurement.

| Band Potential | Mulliken EN theory | | Mott-Schottky plots | |
|---|---|---|---|---|
| | $ZnIn_2S_4$ | $MoS_2$ | $ZnIn_2S_4$ | $MoS_2$ |
| $E_{VB}$ | 1.71 | 1.84 | 1.81 | 1.89 |
| $E_{CB}$ | -1.10 | -0.12 | -1.00 | -0.07 |

[4] C. Du, B. Yan, Z. Lin, G. Yang, Enhanced carrier separation and increased electron density in 2D heavily N-doped $ZnIn_2S_4$ for photocatalytic hydrogen production, *J. Mater. Chem. A*, 2020, **8**, 207.

[5] S. Manchala, V. S. R. K. Tandava, L. R. Nagappagari, S. M. Venkatakrishnan, D. Jampaiah, Y. M. Sabri, S. K. Bhargava, V. Shanker, Fabrication of a novel $ZnIn_2S_4$/g-$C_3N_4$/graphene ternary nanocomposite with enhanced charge separation for efficient photocatalytic $H_2$ evolution under solar light illumination, *Photochem. Photobiol.* Sci., 2019, 18, 2952

[6] D.F. Eaton, Recommended methods for fluorescence decay analysis, *Pure & Appl. Chem.,* 1990, **62(8)**, 1631-1648.

**Table S3.** Comparison of the photocatalytic $H_2$ production rates of the $ZnIn_2S_4/WS_2$ photocatalyst with the previous literature reports.

| Photocatalyst | Weight (mg) | Synthesis method | Light source details | Sacrificial reagent | $H_2$ production rate ($\mu mol\ h^{-1}\ g^{-1}$) |
|---|---|---|---|---|---|
| $ZnIn_2S_4/MoS_2$ (Our work) | 100 | Microwave heating method | 150 W Xe lamp ($\lambda > 400$ nm) | $Na_2S/Na_2SO_3$ | 200.1 |
| Ref. [23] | 50 | Hydrothermal method | 300 W Xe lamp ($\lambda > 420$ nm) | $Na_2S/Na_2SO_3$ | 120 |
| Ref. [7] | 50 | Impregnation method, followed by calcination | 300 W Xe lamp ($\lambda > 420$ nm) | $Na_2S/Na_2SO_3$ | 306 |
| Ref. [22] | 80 | Solvothermal method | 300 W Xe lamp ($\lambda > 420$ nm) | Lactic acid | 2,512.5 |
| Ref. [21] | 80 | Solvothermal method | 300 W Xe lamp ($\lambda > 420$ nm) | $Na_2S/Na_2SO_3$ | 3,891.6 |
| Ref. [24] | 80 | Hydrothermal method | 300 W Xe lamp ($\lambda > 420$ nm) | Lactic acid | 4,287.5 |
| Ref. [25] | 100 | Hydrothermal method | 300 W Xe lamp ($\lambda > 420$ nm) | Lactic acid | 8,047 |

**References**


[7] L. Wei, Y. Chen, Y. Lin, H. Wu, R. Yuan, Z. Li, *Appl. Catal. B.,* 2014, **144**, 521-527.

[21] Z. Zhang, L. Huang, J. Zhang, F. Wang, Y. Xie, X. Shang, Y. Gu, H. Zhao, X. Wang, *Appl. Catal. B.*, 2018, **233**, 112-119.

[22] C. Liu, B. Chai, C. Wang, J. Yan, Z. Ren, *Int. J. Hydrog. Energ.*, 2018, **43**, 6977-6986

[23] T. Huang, W. Chen, T. Y. Liu, Q. L. Hao, X. H. Liu, *Powder Tech.*, 2017, **315**, 157-162.

[24] B. Chai, C. Liu, C. Wang, J. Yan and Z. Ren, *Chinese J. Catal.*, 2017, **38**, 2067-2075.

[25] G. Chen, N, Ding, F. Li, Y. Fan, Y. Luo, D. Li, Q. Meng, *Appl. Catal. B.*, 2014, **160-161**, 614-620.


The difference in the $H_2$ production rate presented in Table S3 could be caused by the variation in the photocatalytic conditions such as the power of the light source and type/concentration of sacrificial reagents. [7,8,9] In addition, the characteristic of the

[7] V. Kumaravel, M. D. Imam, A. Badreldin, R. K. Chava, J. Y. Do, M. Kang, A. Abdel-Wahab, Photocatalytic hydrogen production: role of sacrificial reagents on the activity of oxide, carbon, and sulfide catalysts, *Catalysts*,

photocatalysts that were synthesized via the different methods probably affects the $H_2$ production rate. For the hydrothermal process, $ZnIn_2S_4$ (or $MoS_2$) powder was firstly prepared and then being dispersed in the precursor for $MoS_2$ (or the solution of $Zn^{2+}$, $In^{3+}$ and $S^{2-}$). Finally, the suspension was hydrothermally treated. This strategy could enable the nucleation process of the co-catalyst material on the host material's surface. As a result, the intimate construction of $ZnIn_2S_4/MoS_2$ heterostructure could be achieved, facilitating the interfacial charge transportation in the heterostructure. Although the activity of the $ZnIn_2S_4/MoS_2$ heterostructure prepared in this work is relative low, it exhibits the enhanced photocatalytic activity than that of $ZnIn_2S_4$ or $MoS_2$ for both $H_2$ production and Cr(VI) reduction reactions. Besides, the benefit of the proposed microwave heating synthesis is the reduction in the reaction time and energy consumption for the synthesis of photocatalytic materials.

2019, **9**, 276 (1-35).

[8] B. Weng, M. Qi, C. Han, Z. Tang, Y. Xu, Photocorrosion inhibition of semiconductor-based photocatalysts: basic principle, current development, and future perspective, *ACS Catalysis*, 2019, **9(5)**, 4642-4687.

[9] D. Zhang, J. Cheng, F. Shi, Z. Cheng, X. Yang, M. Cao, Low-temperature synthesis of ribbon-like orthorhombic $NaNbO_3$ fibers and their photocatalytic activities for $H_2$ evolution, *RSC Adv.,* 2015, **5**, 33001-33007.